Highly Sensitive Polymer Based Fabry-Perot Interferometer for Temperature Sensing

Lashari G. Abbas[1, 2], Farhan Mumtaz[1, 2, 3, *], Yutang Dai[1, *], Ai Zhou[1], Wenbin Hu[1], and Muhammad A. Ashraf[3]

Abstract—A highly sensitive temperature sensor based on a polymer cavity of a Fabry-Perot interferometer (FPI) is experimentally demonstrated. The interferometer gives ease in fabrication, and it can be formed by the induction of a thermos-sensitive polymer layer in between two single mode fibers (SMFs). The polymer is used as an FPI cavity for temperature sensing. Due to high thermal expansion coefficient (TEC) and thermos-optic coefficient (TOC) of polymer make the interferometer highly sensitive to ambient temperature. The maximum temperature sensitivity of 2.2209 nm/°C for the polymer FPI cavity of 40.61 µm in the ambient temperature range of 28°C to 34°C is obtained. The proposed sensor shows the advantages of high sensitivity, compactness, simple fabrication, and low cost. Thus, it may become a part of various practical applications in the field of environmental science and engineering sciences.

1. INTRODUCTION

Nowadays, temperature sensors based on optical fiber are getting fame because of their tiny size, light weight, low cost, high sensitivity, robustness, immunity to electromagnetic interference, and ability to sustain in harsh environments. Their deployment in various engineering models have been established. In last decade, several fiber optic sensors have been realized and reported for temperature sensing. These interferometers include Fiber Brag Grating (FBG) [1–4], Long-Period Fiber Grating (LPFG) [5–8], Mode field interferometers [9, 10], Mach-Zehnder Interferometers (MZI) [11–16], Michelson Interferometers (MI) [17, 18], Fabry-Perot Interferometers (FPI) [19–23], Hybrid Interferometers (MZI and FPI) [12, 14, 24], Interferometer composed of Silicon-on-Insulators (SOI) [25], and Surface Plasma Resonance (SPR) [26]. In these configurations, mostly silica is used as a sensing element for temperature measurement. Since pure silica attaind the properties of extremely low TOC and TEC, as a result such structures exhibit low temperature sensitivity. Alternatively, those structures composed of SOI are relatively highly sensitive to ambient temperature because of their high TEC and TOC. On the other hand, these structures show the constraints of coupling deficiencies and are expensive. SPRs are also famous in interferometry for their highly sensitive response to temperature. They can be fabricated by pouring nanoparticles [27] into the hollow cores of photonic crystal fibers (PCF) [28] or depositing the nano-films [29, 30] on a special optical fiber. However, these structures involve multiple complexities during fabrication, and expensive devices are also reported.

Several methods and designs have been proposed to enhance the sensitivity of fiber optic temperature sensors so that they can meet the needs of modern applications. One of the prominent methods is micro-machining that is used to form tapered fiber, and this process makes the structure

known as microfiber. In tapered fibers, a large evanescent field is generated by an interferometer. Such structures significantly enhance the sensitivity compared to the ordinary silica-based fiber structures [27, 29]. It is also noticed that these microfiber structures are fragile, and their fabrication steps involve complexities, i.e., tools align, accuracy, etc. These limitations halt the usage of such interferometer in practical applications. Several conventional optical fiber sensors have been reported that are constituted by coating thermos-sensitive materials [10, 11, 19, 29], i.e., graphene [29], metals [15], polymers [4, 29], etc. However, these structures are composed of Hollow Core Fiber (HCF) used for the design of high sensitivity devices [21]. In the composition of HCF structures, high TOC of polymer is filled into the air holes of HCF to make the interferometer highly sensitive to environment, whereas their fabrication procedure is quite simple, easy, and cost-effective. However, HCF based sensors show the disadvantage of low mechanical strength due to fragility.

In the era of modern applications, there is a need to develop such kind of temperature sensors that are easy to fabricate, highly compact, highly sensitive, and economical. In order to meet the current requirements, a polymer-based temperature sensor is proposed for measuring the ambient temperature response. The proposed sensor is simple in structure, highly sensitive, compact, and cost-effective. It also provides high temperature sensitivity at room temperature which makes it a suitable choice for many practical applications. In composition, the maximum FPI cavity of 60 μm is used in the proposed structure. In such a way, it can be easily embedded into various devices. The structure is formed by the placement of Ultraviolet (UV) curable Norland Optical Adhesive 65 (NOA65) in between two SMFs. The proposed FPI design is inexpensive that involves simple techniques of cleaving, patching of the SMF with transparent polymer, and UV curing. Whereas, the transparent photopolymer has high TEC and TOC, thus, it provides high temperature sensitivity.

The rest of the article is organized as follows. Section 2 describes the fabrication and theoretical analysis of the proposed FPI temperature sensor. Experimental results are presented in Section 3.

2. SENSOR FABRICATION AND THEORETICAL ANALYSIS

2.1. Fabrication

The schematic diagram of the proposed FPI temperature sensor is illustrated in Fig. 1. It comprises SMF-1 and SMF-2, and a thermos-sensitive polymer layer is placed in between them. The SMF (corning-28) is used with the core diameter of 8.2 μm and the cladding diameter of 125 μm. The thermos-sensitive polymer is of adhesive type which is also known as Norland Optical Adhesive 65 (NOA65). The polymer is a transparent liquid photopolymer which can be easily transformed into solid state, when ultraviolet (UV) light is illuminated on it. The refractive index of NOA65 polymer is 1.52 in solid state.
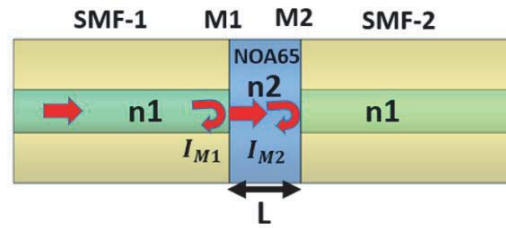

Figure 1. Schematic diagram of the FPI temperature sensor.

The proposed FPI sensor is used to fabricate with a cost effective procedure. In fabrication, simple steps of cleaving, aligning, and UV curing are utilized to constitute the FPI temperature sensor. The proposed sensor can be fabricated by the following steps. Step 1: SMF-1 and SMF-2 are cleaved with the help of a high precision cleaver, as shown in Fig. 2(a). Step 2: the cleaved facets of SMF-1 and SMF-2 are immersed into NOA65 adhesive solution for 30 seconds so that adhesive solution can deposit on the end facets of each SMF, and deposition may occur due to capillary action, as shown in Fig. 2(b). Step 3: SMF-1 and SMF-2 with NOA65 at their end facets are then placed on ordinary fusion splicing machine. The manual mode function in the splicer menu is used to align the deployed SMFs
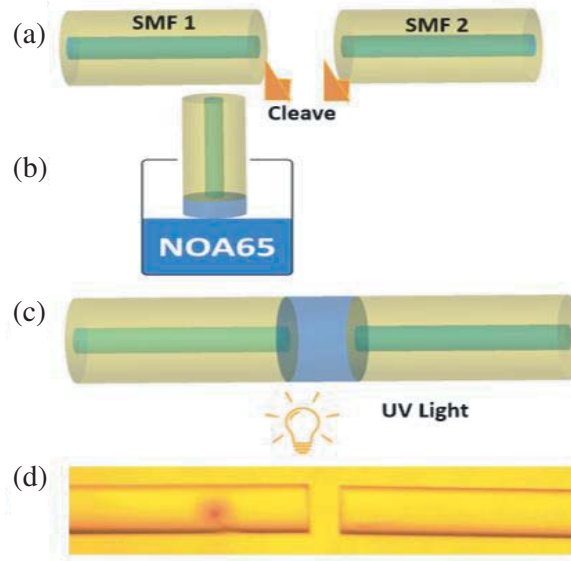
Figure 2. Fabrication steps of the proposed polymer based on FPI cavity temperature sensor.

until both of NOA65 intact with each other. Here, one thing is ensured that no splicing program is to preform through fusion splicer. Then UV point source light illuminates the optical adhesive solution for the solidification of NOA65 polymer. UV LED light curing equipment (FUV-6BK) is used to illuminate UV light on the adhesive solution for about 30 minutes, as shown in Fig. 2(c). As a result, the NOA65 is turned into a solid transparent photopolymer, and subsequently this process constitutes a polymer based FPI cavity in the proposed temperature sensor. NOA65 is a type of transparent liquid photopolymer that can be easily converted into a solid state polymer when it is exposed to UV light. In the solidification of polymer, the UV light of wavelength from 350 nm to 380 nm is used. The micrograph of the polymer based on an FPI cavity temperature sensor is illustrated in Fig. 2(d). NOA65 polymer is transparent in nature and is not visible in micrograph, whereas SMF-1 and SMF-2 can be seen in Fig. 2(d). This micrograph is recorded by Light Polarized Microscope (LT/UPR203i). This microscope is equipped with a charged coupled device (CCD) camera which is integrated with PC to record micro-graph images.

2.2. Working Principle

The optical paths of proposed polymer based on FPI cavity temperature sensor is shown in Fig. 1. The incident light coming from SMF-1 propagates through photosensitive polymer NOA65, and eventually it experiences Fresnel reflection at M_1 mirror. Here, a portion of the light reflects back while the remaining part of light propagates through the photosensitive polymer NOA65. When the light reaches the facet of SMF-2, a portion of light again reflects back from M_2 mirror. Thus, the reflection from M_1 and M_2 forms a dual beam interference in the polymer cavity. The total reflection intensity of two beams I_{M1} and I_{M2} can be expressed as,

$$I = I_{M1} + I_{M2} + 2\sqrt{I_{M1} \cdot I_{M2}} \cos(\theta) \tag{1}$$

where θ is the phase difference of the light beams which can be expressed as,

$$\theta = \frac{4\pi n_2 L}{\lambda} \tag{2}$$

where λ is the wavelength of the input light. n_2 is the effective refractive index of the polymer (NOA65), and L is the sensing length of the polymer cavity. The phase difference satisfies the following condition as,

$$\theta = (2m+1)\pi; \quad \text{for } m = 0, 1, 2, \ldots \tag{3}$$

Then, the resonant dips will appear in the wavelength as,

$$\lambda_{dip}^m = \frac{4\pi n_2 L}{(2m+1)\pi}, \quad m = 0, 1, 2, \ldots \tag{4}$$

When ambient temperature changes, the FPI cavity of polymer NOA65 expands and contracts with temperature increase or decrease, respectively. As a result, sufficient change in the length of the polymer cavity is expected due to high TEC and TOC with temperature change. Therefore, the corresponding wavelength causes shift with temperature rise or fall, and the sensitivity of device can be theoretically measured as,

$$S = \frac{\partial \lambda}{\partial T} = \lambda_{dip}^m (\alpha + \xi), \quad m = 0, 1, 2, \ldots \tag{5}$$

where α and ξ are the TEC and TOC of the polymer, respectively. The value of α for NOA65 is about $2.25 \times 10^{-4}/°C$, whereas the value of ξ is $-1.17 \times 10^{-4}/°C$ at 25°C–55°C, and $\xi = 1/\Delta n \cdot \partial n/\partial T$, where the change in refractive index is negligible which is ignored in the analysis. The polymer based on pure silica has low TEC and TOC, and subsequently all-fiber FPI cavities of pure silica polymer present low sensitivities. However, highly thermos-sensitive polymer material for designing FPI cavity can drastically enhance the sensitivity of devices. In order to ensure the highly temperature sensitive device, a polymer based on FPI cavity sensor is proposed with high TEC and TOC.

3. EXPERIMENTAL RESULTS

In experimental investigations, two different samples of polymer-based on FPI cavity temperature sensors are fabricated. The sensing lengths of polymer based FPI cavity are taken as 59.67 μm and 40.61 μm for two different sensors of sample 1 (S1) and sample 2 (S2), respectively. These sensors are used to study the ambient temperature shift in detail. The experimental setup for measuring the temperature response is shown in Fig. 3. In order to study the ambient temperature, the proposed sensor is kept in a thermoelectric container, whose measuring error is about 0.01°C. In Fig. 3, the inset elaborates the design of the temperature sensor based on a polymer FPI cavity. Besides, a thermometer probe is also placed into the thermoelectric container to cross-monitoring in case of the temperature shift. An Amplified Spontaneous Emission (ASE) source of broadband wavelength range from 1520 nm to 1600 nm is employed to trace the interference dips. A 3 dB optical coupler is employed to recombine the reflected light beams, and the reflection spectrum is monitored by using an optical spectrum analyzer (OSA). The wavelength resolution of the OSA is set to 0.02 nm.

In the construction of FPIs, UV curable adhesive material is used, whereas the adhesive material has much higher TEC than silica. Firstly, S1 is placed into the thermoelectric container. The Free Spectral Range (FSR) and the interference fringe visibility for S1 are measured as 13 nm and 8 dB, respectively,
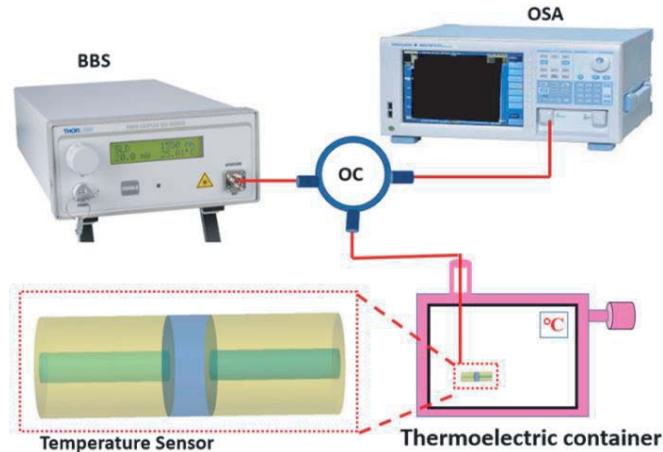

Figure 3. Temperature measurement setup for FPI sensor.

shown in Fig. 4. The spectral shift response of S1 sensor is observed for ambient temperature shift from 28°C to 34°C with a step of 1°C. It is observed during investigation that when the temperature rises, the thermos-sensitive polymer expands. Resultantly, the FPI cavity length increases with temperature rise. Thus, resonant dips of the sensor show read-shift with temperature rise. The shifting of wavelength spectra with temperature rise is shown in Fig. 5. Sensor S1 exhibits the temperature sensitivity of 1.0027 nm/°C with a high linearity correlation of 0.9995, as shown in Fig. 6. These ambient temperature measurements are consistent with theoretical data which are subject to measurement errors.

The same experimental setup, as shown in Fig. 3, is used to measure the temperature response of S2. For sensor S2, the FSR and interference fringe visibility are measured as 20 nm and 8 dB, respectively, shown in the Fig. 7. The spectral evolution of S2 is obtained at the ambient temperature range from 28°C to 34°C with an increasing step of 1°C. The spectral evolution with temperature rise is recorded which is shown in Fig. 8. The sensor S2 exhibits the temperature sensitivity of 2.2209 nm/°C with a high linearity correlation of 0.9991, as shown in Fig. 9. The experimental results indicate that a shorter length FPI cavity possesses high sensitivity, which is consistent with theoretical analysis subject to measurement errors. The obtained sensitivities and FSR in respect of S1 and S2 are listed in Table 1. A detail comparison is made with earlier reported sensors with respective to their sensitivities, which
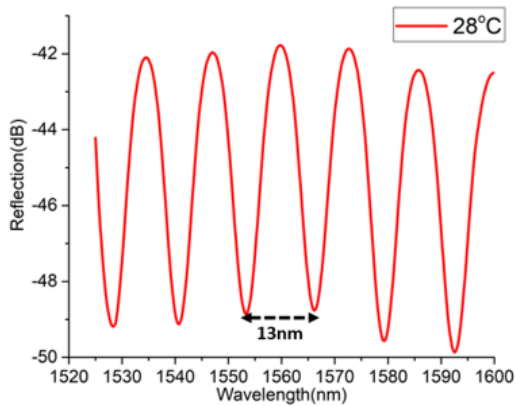

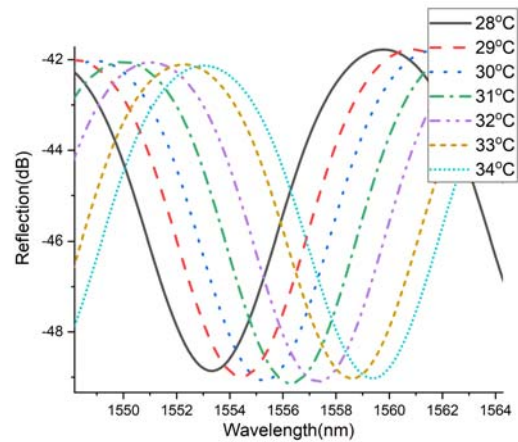**Figure 4.** Spectrum of the temperature sensor sample (S1).

Figure 5. Reflection spectral evolution of FPI sensor (S1) under different temperature measurements.
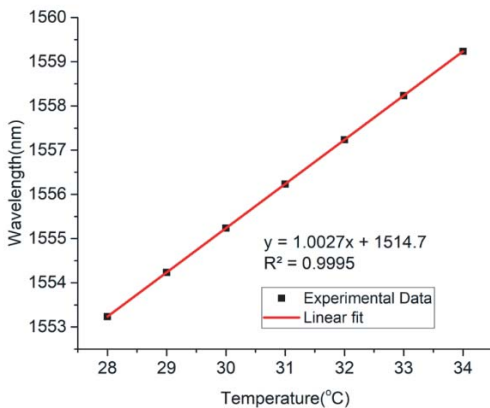

Figure 6. Linear fitting line for wavelength versus temperature (S1).
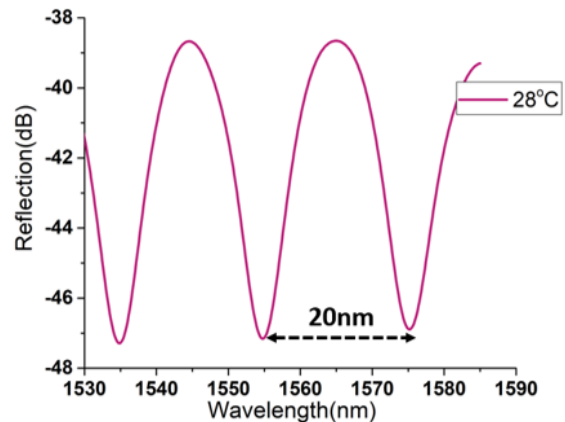

Figure 7. Spectrum of the temperature sensor sample (S2).

is listed in Table 2. This comparison indicates that polymer based proposed sensor can effectively enhance the temperature sensitivity with a simple approach of fabrication and easy handling. The proposed sensing architecture is inexpensive, which may play a vital role to become a part of different practical applications.
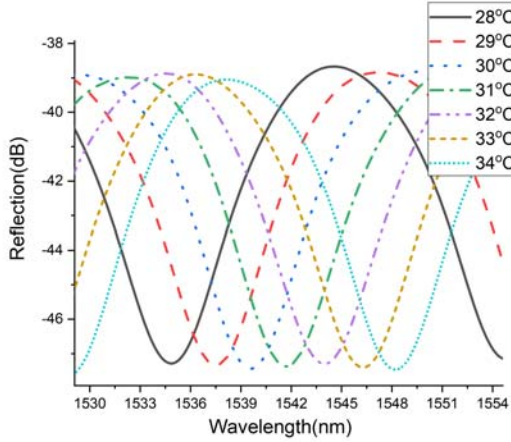

Figure 8. Reflection spectral evolution of FPI sensor (S2) under different temperature measurements.
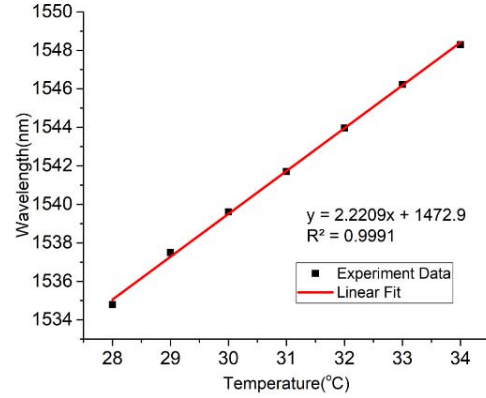

Figure 9. Linear fitting line for wavelength versus temperature (S2).

Table 1. FSR and sensitivity of two tested samples.

S1	S2	Parameters
13	20	Sensing FSR (nm)
1.0027	2.2209	Sensitivity (nm/$^\circ$C)

Table 2. Sensitivity and structure of some temperature sensors.

Reference	Sensor Structure	Sensitivity (pm/$^\circ$C)
[3]	Polished SMF end face	13.32 pm/$^\circ$C
[31]	PCF-SMF offset	13 pm/$^\circ$C
[32]	Polystyrene-coated fiber tip	439.9 pm/$^\circ$C
[33]	Ultraviolet curing Glue	223.4 pm/$^\circ$C
[6]	Polymer based	385.8 pm/$^\circ$C
[17]	Microsphere array	115.3 pm/$^\circ$C
[18]	Large core-offset	9.5 pm/$^\circ$C
[34]	TCF-SHF cascaded	10.37 pm/$^\circ$C
[11]	Polymer based	101 pm/$^\circ$C
[4]	Polymer based	307.6 pm/$^\circ$C
This work	Polymer cavity	2.2209 nm/$^\circ$C

4. CONCLUSION

In this paper, a highly sensitive temperature sensor based on a polymer FPI cavity is developed and experimentally tested. The interferometer is simple in design and is constituted by the placement of thermos-sensitive polymer in between SMFs. The polymer FPI cavity is found highly sensitive

to ambient temperature because of high TEC and TOC. The maximum temperature sensitivities of $2.2209\,\mathrm{nm/°C}$ and $1.0027\,\mathrm{nm/°C}$ have been achieved for S1 and S2 with high linear correlations. The proposed FPI sensing architecture has many advantages, i.e., high sensitivity, compact size, ease of fabrication, and above all cost-effectiveness. Therefore, it can be a right choice for plenty of practical applications in different fields of engineering and natural sciences.

REFERENCES

1. Mumtaz, F., et al., "A design of taper-like etched multicore fiber refractive index-insensitive a temperature highly sensitive Mach-Zehnder interferometer," *IEEE Sensors Journal*, Vol. 20, No. 13, 7074–7081, 2020.
2. Li, X., L. V. Nguyen, M. Becker, H. Ebendorff-Heidepriem, D. Pham, and S. Warren-Smith, "Simultaneous measurement of temperature and refractive index using an exposed core microstructured optical fiber," *IEEE Journal of Selected Topics in Quantum Electronics*, Vol. 26, No. 4, 1–7, 2019.
3. Yu, J., S. Xu, Y. Jiang, H. Chen, and W. Feng, "Multi-parameter sensor based on the fiber Bragg grating combined with triangular-lattice four-core fiber," *Optik*, Vol. 208, 164094, 2020.
4. Zhang, W., Y. Liu, T. Zhang, D. Yang, Y. Wang, and D. Yu, "Integrated fiber-optic Fabry-Perot interferometer sensor for simultaneous measurement of liquid refractive index and temperature," *IEEE Sensors Journal*, Vol. 19, No. 13, 5007–5013, 2019.
5. Cao, X., D. Tian, Y. Liu, L. Zhang, and T. Wang, "Sensing characteristics of helical long-period gratings written in the double-clad fiber by CO2 laser," *IEEE Sensors Journal*, Vol. 18, No. 18, 7481–7485, 2018.
6. Li, Z., Y.-X. Zhang, W.-G. Zhang, L.-X. Kong, and T.-Y. Yan, "Micro-cap on 2-core-fiber facet hybrid interferometer for dual-parameter sensing," *Journal of Lightwave Technology*, Vol. 37, No. 24, 6114–6120, 2019.
7. Rao, Y.-J., Y.-P. Wang, Z.-L. Ran, and T. Zhu, "Novel fiber-optic sensors based on long-period fiber gratings written by high-frequency CO2 laser pulses," *Journal of Lightwave Technology*, Vol. 21, No. 5, 1320, 2003.
8. Zheng, Z.-M., Y.-S. Yu, X.-Y. Zhang, Q. Guo, and H.-B. Sun, "Femtosecond laser inscribed small-period long-period fiber gratings with dual-parameter sensing," *IEEE Sensors Journal*, Vol. 18, No. 3, 1100–1103, 2017.
9. Tian, K., et al., "Simultaneous measurement of displacement and temperature based on two cascaded balloon-like bent fibre structures," *Optical Fiber Technology*, Vol. 58, 102277, 2020.
10. Yi, D., Z. Huo, Y. Geng, X. Li, and X. Hong, "PDMS-coated no-core fiber interferometer with enhanced sensitivity for temperature monitoring applications," *Optical Fiber Technology*, Vol. 57, 102185, 2020.
11. Gong, J., et al., "High sensitivity fiber temperature sensor based PDMS film on Mach-Zehnder interferometer," *Optical Fiber Technology*, Vol. 53, 102029, 2019.
12. Huang, B., et al., "In-fiber Mach-Zehnder interferometer exploiting a micro-cavity for strain and temperature simultaneous measurement," *IEEE Sensors Journal*, Vol. 19, No. 14, 5632–5638, 2019.
13. Lei, X., Y. Feng, and X. Dong, "High-temperature sensor based on a special thin-diameter fiber," *Optics Communications*, Vol. 463, 125386, 2020.
14. Tong, R.-J., Y. Zhao, H.-K. Zheng, and F. Xia, "Simultaneous measurement of temperature and relative humidity by compact Mach-Zehnder interferometer and Fabry-Perot interferometer," *Measurement*, Vol. 155, 107499, 2020.
15. Wang, J., C. Bian, T. Gang, and M. Hu, "High-sensitive Mach-Zehnder interferometer for humidity measurements based on concatenating single-mode concave cone and core-offset," *Optik*, Vol. 208, 164465, 2020.
16. Wang, Z., L. Huang, C. Liu, H. Wang, S. Sun, and D. Yang, "Sensitivity-enhanced fiber temperature sensor based on vernier effect and dual in-line Mach-Zehnder interferometers," *IEEE Sensors Journal*, Vol. 19, No. 18, 7983–7987, 2019.

17. Qi, K., Y. Zhang, J. Sun, G. J. O. Yi, and L. Technology, "All-fiber high temperature and refractive index sensor based on three microspheres array Michelson interferometer," *Optics Laser Technology*, Vol. 129, 106300, 2020.

18. Sun, H., M. Shao, L. Han, J. Liang, R. Zhang, and H. Fu, "Large core-offset based in-fiber Michelson interferometer for humidity sensing," *Optical Fiber Technology*, Vol. 55, 102153, 2020.

19. Domínguez-Flores, C. E., et al., "Real-time temperature sensor based on in-fiber Fabry–Perot interferometer embedded in a resin," *Journal of Lightwave Technology*, Vol. 37, No. 4, 1084–1090, 2019.

20. Lei, X. and X. Dong, "High-sensitivity Fabry-Perot interferometer high-temperature fiber sensor based on vernier effect," *IEEE Sensors Journal*, Vol. 20, No. 10, 5292–5297, 2020.

21. Liu, Y., et al., "Hollow-core fiber-based all-fiber FPI sensor for simultaneous measurement of air pressure and temperature," *IEEE Sensors Journal*, Vol. 19, No. 23, 11236–11241, 2019.

22. Yang, D., et al., "Integrated optic-fiber sensor based on enclosed EFPI and structural phase-shift for discriminating measurement of temperature, pressure and RI," *Optics Laser Technology*, Vol. 126, 106112, 2020.

23. Zhu, C., Y. Zhuang, B. Zhang, R. Muhammad, P. P. Wang, and J. Huang, "A miniaturized optical fiber tip high-temperature sensor based on concave-shaped Fabry-Perot cavity," *IEEE Photonics Technology Letters*, Vol. 31, No. 1, 35–38, 2018.

24. Cheng, H., S. Wu, Q. Wang, S. Wang, and P. Lu, "In-line hybrid fiber sensor for curvature and temperature measurement," *IEEE Photonics Journal*, Vol. 11, No. 6, 1–11, 2019.

25. Xu, H., M. Hafezi, J. Fan, J. M. Taylor, G. F. Strouse, and Z. Ahmed, "Ultra-sensitive chip-based photonic temperature sensor using ring resonator structures," *Optics Express*, Vol. 22, No. 3, 3098–3104, 2014.

26. Liu, Y., S. Li, H. Chen, J. Li, W. Zhang, and M. Wang, "Surface plasmon resonance induced high sensitivity temperature and refractive index sensor based on evanescent field enhanced photonic crystal fiber," *Journal of Lightwave Technology*, Vol. 38, No. 4, 919–928, 2019.

27. Bai, Y., Y. Miao, H. Zhang, and J. Q. Yao, "Simultaneous measurement of temperature and relative humidity based on a microfiber sagnac loop and MoS2," *Journal of Lightwave Technology*, Vol. 38, No. 4, 840–845, 2020.

28. Yin, J., et al., "Assembly-free-based fiber-optic micro-Michelson interferometer for high temperature sensing," *IEEE Photonics Technology Letters*, Vol. 28, No. 6, 625–628, 2015.

29. Hernández-Romano, I., D. Monzón-Hernández, C. Moreno-Hernández, D. Moreno-Hernandez, and J. Villatoro, "Highly sensitive temperature sensor based on a polymer-coated microfiber interferometer," *IEEE Photonics Technology Letters*, Vol. 27, No. 24, 2591–2594, 2015.

30. Li, J.-X., Z.-R. Tong, L. Jing, W.-H. Zhang, J. Qin, and J.-W. J. O. C. Liu, "Fiber temperature and humidity sensor based on photonic crystal fiber coated with graphene oxide," *Optics Communications*, Vol. 467, 125707, 2020.

31. Sun, H., et al., "A hybrid fiber interferometer for simultaneous refractive index and temperature measurements based on Fabry-Perot/Michelson interference," *IEEE Sensors Journal*, Vol. 13, No. 5, 2039–2044, 2013.

32. Salunkhe, T. T., D. J. Lee, H. K. Lee, H. W. Choi, S. J. Park, and I. T. Kim, "Enhancing temperature sensitivity of the Fabry-Pérot interferometer sensor with optimization of the coating thickness of polystyrene," *Sensors*, Vol. 20, No. 3, 794, 2020.

33. Liu, Y., et al., "Fabrication of dual-parameter fiber-optic sensor by cascading FBG with FPI for simultaneous measurement of temperature and gas pressure," *Optics Communications*, Vol. 443, 166–171, 2019.

34. Zhao, Y., et al., "An integrated fiber michelson interferometer based on twin-core and side-hole fibers for multiparameter sensing," *Journal of Lightwave Technology,* Vol. 36, No. 4, 993–997, 2017.